Lattice Boltzmann simulations of three-dimensional incompressible flows in a four-sided lid driven cavity

2017 Fluid Dyn. Res. 49 025507

(http://iopscience.iop.org/1873-7005/49/2/025507)

IOP Publishing | The Japan Society of Fluid Mechanics Fluid *Dynamics* Research

Fluid Dyn. Res. **49** (2017) 025507 (18pp) https://doi.org/10.1088/1873-7005/aa5658

Lattice Boltzmann simulations of three-dimensional incompressible flows in a four-sided lid driven cavity

Cheng Gong Li[1] **and Jerome P-Y Maa**[2]

[1] National Engineering Laboratory for MTO, Dalian National Laboratory for Clean Energy, Dalian Institute of Chemical Physics, Chinese Academy of Sciences, 457 Zhongshan Road, Dalian 116023, People's Republic of China
[2] Virginia Institute of Marine Science, College of William & Mary, Gloucester Point, VA 23062, United States

E-mail: chenggongli@dicp.ac.cn

Received 5 July 2016, revised 3 December 2016
Accepted for publication 3 January 2017
Published 6 February 2017

Communicated by Masahito Asai

Abstract

Numerical study on three-dimensional (3D), incompressible, four-sided lid (FSL) driven cavity flows has been conducted to show the effects of the transverse aspect ratio, K, on the flow field by using a multiple relaxation time lattice Boltzmann equation. The top wall is driven from left to right, the left wall is moved downward, whereas the right wall is driven upward, and the bottom wall is moved from right to left, all the four moving walls have the same speed and the others boundaries are fixed. Numerical computations are performed for several Reynolds numbers for laminar flows, up to 1000, with various transverse aspect ratios. The flow can reach a steady state and the flow pattern is symmetric with respect to the two cavity diagonals (i.e., the center of the cavity). At Reynolds number = 300, the flow structures of the 3D FSL cavity flow at steady state with various transverse aspect ratio, i.e., 3, 2, 1, 0.75, 0.5 and 0.25 only show the unstable symmetrical flow pattern. The stable asymmetrical flow pattern could be reproduced only by increasing the Reynolds number that is above a critical value which is dependent on the aspect ratio. It is found that an aspect ratio of more than 5 is needed to reproduce flow patterns, both symmetric and asymmetric flows, simulated by using 2D numerical models.

Keywords: 3D four-sided lid driven cavity flow, transverse aspect ratio, multiple relaxation time lattice Boltzmann equation (MRT-LBE), laminar flow

(Some figures may appear in colour only in the online journal)

1. Introduction

Vortex in a cavity flow where the fluid motion is driven by the selected moving wall boundaries is an important benchmark study (Ghia *et al* 1982). The significance of this problem is due to its industrial contexts, e.g., short-dwell coater and in melt spinning process for production of microcrystalline material, and scientific research because it exhibits almost all phenomena that possibly occur in incompressible flows: eddies, secondary flows, Taylor-Görtler-like vortices, flow bifurcations, instabilities, transition, and turbulence. Thus, lid driven cavity (LDC) flows have been studied extensively by numerical simulations (Burggraf 1966, Pan and Acrivos 1967, Ghia *et al* 1982, Chiang *et al* 1998, Shankar and Deshpande 2000) and laboratory experiments (Koseff and Street 1984a, 1984b and 1984c, Prasad and Koseff 1989, Guermond *et al* 2002).

The pioneering analytical and numerical studies of this type flows were given by Burggraf (1966) who computed steady flows driven by a uniform translation of the top wall and by Pan and Acrivos (1967) who examined the flow structure experimentally by using a photographic technique for two-dimensional (2D) rectangular cavities, but neglected the three dimensional (3D) effects on the flow patterns. Experiments on circulation pattern of 3D cavity flow with only one side is moving (hereafter call one-sided cavity flow) with various aspect ratios (see section 3 for definition) was comprehensively reported for the effects of the end wall on the fluid motion (Koseff and Street 1984a, 1984b and 1984c, Prasad and Koseff 1989). In particular, a detailed review on 2D and 3D one-sided cavity flow has been presented by Shankar and Deshpande (2000).

Two-sided cavity flow which is driven by the parallel (or perpendicular) motion of two facing (or perpendicular) walls in 3D rectangular cavity with various aspect ratios, was firstly investigated experimentally and numerically by Kuhlmann *et al* (1997), among others (Albensoeder *et al* 2001, Blohm and Kuhlmann 2002). The results showed that a multiplicity of flow patterns/states may occur because of the difference in aspect ratio and the Reynolds number. Recently, a 2D two-sided cavity flow which is driven by the non-facing moving walls for a square cavity and the 2D four-sided lid (FSL) driven cavity flow were reported by Wahba (2009) to examine the multiple solutions and the Reynolds number for flow bifurcation. A total of three (one unstable symmetric and two stable asymmetric) solutions are captured. The stability analysis of these three flow patterns was performed by Cadou *et al* (2012). To analyze the 3D flow motion and estimate the 3D effects on the flow structure, the two-sided non-facing lid (TSNFL) driven cavity flow has been extended to 3D by Beya and Lili (2008) and Oueslati *et al* (2011).

Even though the FSL cavity flow was investigated numerically for its multiple solutions in two dimensions at low Reynolds number (De *et al* 2009, Wahba 2009), corresponding study in 3D has not been done. For 3D FSL, the top wall is driven from left to right, the left wall is moved downward, whereas the right wall is driven upward, and the bottom wall is moved from right to left, all the four moving walls have the same speed and the others boundaries are fixed. In this study, lattice Boltzmann method (LBM) is used to simulate all the 3D fluid flows. In contrast to the conventional numerical solution of macroscopic equation, i.e., Navier–Stokes equation (NSE), LBM solves the macroscopic averaged properties and the evolution of the statistical distribution of microscopic particles in term of the discrete kinetic theory. The advantages of using LBM include easy implementation of boundary conditions, short codes, and natural parallelism (Succi 2001). Thus, LBM has been

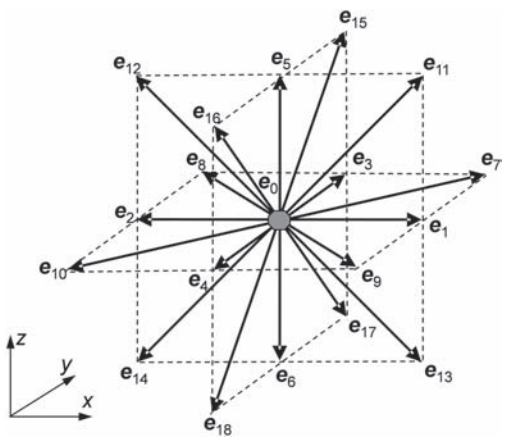

Figure 1. The schematic of D3Q19 model for MRT at any node, $\boldsymbol{r}_i$, and the 19 velocities, $\boldsymbol{e}_\alpha$, with $\alpha = 0, 1, \ldots, 18$.

developed into an effective computational tool for simulating many complex fluid problems, such as multiphase flows, porous media, turbulent flows, etc (Gunstensen *et al* 1991, Hou *et al* 1995, 1996, Dardis and Mccloskey 1998, Li *et al* 2012). Recently, multiple-relaxation time (MRT) LBE was proposed for improving the numerical stability (d'Humières 1992, Lallemand and Luo 2000). It has been proved that the numerical stability of MRT-LBE is indeed superior to that of early version of LBE for simulating 3D cavity flows (d'Humières *et al* 2002).

The objectives of this study are to (a) simulate 3D FSL cavity flows and the effects of transverse aspect ratio on the flow structure at steady states, (b) and capture the multiplicity of steady solutions in 3D situation. To this end, the MRT-LBE with 3D nineteen velocity directions (D3Q19) model is adopted, and the results are compared with other numerical methods that solved the NSE.

The remaining part of this study is organized as follows. In section 2, the numerical model of D3Q19 MRT-LBE is introduced briefly. In section 3, detailed results from MRT-LBE model for the 3D FSL cavity flow are presented and analyzed. Finally, conclusions are provided in section 4.

2. Numerical model

2.1. Multiple relaxation time lattice Boltzmann equation

The evolution equation of MRT-LBE (also called the generalized LBE or the moment method) for M velocity directions in the D-dimensional space can be written as (d'Humières *et al* 2002)

$$f_\alpha(\boldsymbol{x}_i + \boldsymbol{e}_\alpha \Delta t, t + \Delta t) - f_\alpha(\boldsymbol{x}_i, t) = -(M^{-1}SM)_{\alpha\beta}[f_\beta(\boldsymbol{x}_i, t) - f_\beta^{(\mathrm{eq})}(\boldsymbol{x}_i, t)]. \tag{1}$$

Here, the right hand side of the equation (1) describes the particle collision process, the left hand side represents the particle streaming process from the node $\boldsymbol{x}_i$ to the nearest neighbor node $\boldsymbol{x}_i + \boldsymbol{e}_\alpha \Delta t$ during one time step interval Δt with a velocity $\boldsymbol{e}_\alpha$ along the corresponding direction α. In equation (1), f_α ($\boldsymbol{x}_i$, t) indicates the particle distribution function at the location $\boldsymbol{x}_i$ and time t associated with the discrete particle velocities $\boldsymbol{e}_\alpha$, and its moments are related to

the local macroscopic velocity $\boldsymbol{u}$ and density ρ as follows

$$\rho = \sum_{\alpha} f_{\alpha}, \quad \rho \boldsymbol{u} = \sum_{\alpha} \boldsymbol{e}_{\alpha} f_{\alpha}. \tag{2}$$

In this study, we used the nineteen velocity model on three dimension cubic lattices (D3Q19 model, see figure 1), and thus, the discrete particles velocities $\boldsymbol{e}_{\alpha}$ are defined as (d'Humières *et al* 2002)

$$\boldsymbol{e}_{\alpha} = \begin{cases} c(0, 0, 0) & \alpha = 0, \\ c(\pm 1, 0, 0), c(0, \pm 1, 0), c(0, 0, \pm 1) & \alpha = 1\text{–}6, \\ c(\pm 1, \pm 1, 0), c(\pm 1, 0, \pm 1), c(0, \pm 1, \pm 1) & \alpha = 7\text{–}18, \end{cases} \tag{3}$$

where $c = \Delta x / \Delta t$ stands for the magnitude of the discrete particle velocity, and Δx is the dimensionless lattice length. For simplicity, Δx and Δt are set equal to 1, that is $c = \delta x = \delta t = 1$.

The corresponding collision matrix, S is given by (d'Humières *et al* 2002)

$$S = \mathrm{diag}(s_0, s_1, s_2, s_3, s_4, s_5, s_6, s_7, s_8, s_9, s_{10}, s_{11}, s_{12}, s_{13}, s_{14}, s_{15}, s_{16}, s_{17}, s_{18}), \tag{4}$$

where s_i ($i = 0, 1, \ldots, 18$) stands for the relaxation rate corresponding to the nineteen directions, $s_0 = s_3 = s_5 = s_7$, $s_2 = s_{10} = s_{12}$, and $s_{16} = s_{17} = s_{18}$. Since the incompressible NSE could be deduced from the GLBE by using the Chapman-Enskog expansion, the viscosity υ which is obtained from this expansion under the condition $s_9 = s_{11} = s_{13} = s_{14} = s_{15} = s_{\upsilon} = 1/\tau$, where τ is the total relaxation time and related to the viscosity, υ, as follows (d'Humières *et al* 2002)

$$\upsilon = c_s^2 (\tau - 0.5) \Delta t. \tag{5}$$

The transformation matrix M linearly transforms the PDFs, f_{α} and the equilibrium PDFs, $f_{\alpha}^{(\mathrm{eq})}$ to the moments, m_{α} and the equilibrium moments $m_{\alpha}^{(\mathrm{eq})}$, that is, (d'Humières *et al* 2002)

$$|m\rangle = (\rho, e, \varepsilon, j_x, q_x, j_y, q_y, j_z, q_z, 3p_{xx}, 3\pi_{xx}, p_{ww}, \pi_{ww}, p_{xy}, p_{yz}, p_{xz}, m_x, m_y, m_z)^T, \tag{6}$$

where ρ stands for the mass density, also can be replaced by density fluctuation $\delta\rho = \rho - \rho_0$ for reducing the effects due to the round-off error in the LBE simulations, e is the kinetic energy, ε is the kinetic energy square, j_x, j_y, and j_z are the three components of the momentum in the x, y, and z directions, respectively, q_x, q_y, and q_z stand for the three components of the energy flux in the x, y, and z directions, respectively, p_{xx} is the dynamic pressure in the x direction, p_{ww} is the dynamic pressure in z direction, p_{xy}, p_{yz}, and p_{xz} are the symmetric traceless viscous stress tensor, $3\pi_{xx}$, $3\pi_{ww}$ are the fourth-order moments, and m_x, m_y, and m_z are the third-order moments (d'Humières *et al* 2002).

For the equilibrium value of moments $m_{\alpha}^{(\mathrm{eq})}$ in D3Q19 model, mass density $m_0^{(\mathrm{eq})} = \rho$, three components of momentum $m_{3,5,7}^{(\mathrm{eq})} = j_{x,y,z}$ are the conserved moments, and others are the non-conserved moments. Thus, the equilibrium PDF, $f_{\alpha}^{(\mathrm{eq})}$ which corresponds to the $m_{\alpha}^{(\mathrm{eq})}$ is defined as

$$f_{\alpha}^{(\mathrm{eq})} = \omega_{\alpha} \rho \left\{ 1 + \frac{\boldsymbol{e}_{\alpha} \cdot \boldsymbol{u}}{c_s^2} + \frac{(\boldsymbol{e}_{\alpha} \cdot \boldsymbol{u})^2}{2c_s^4} - \frac{\boldsymbol{u}^2}{2c_s^2} \right\}, \tag{7}$$

where ω_{α} is the weight parameters, $\omega_0 = 1/3$, $\omega_{1\text{-}6} = 1/18$, $\omega_{7-18} = 1/36$, ${c_s}^2 = c/3$ are the lattice sound speed.

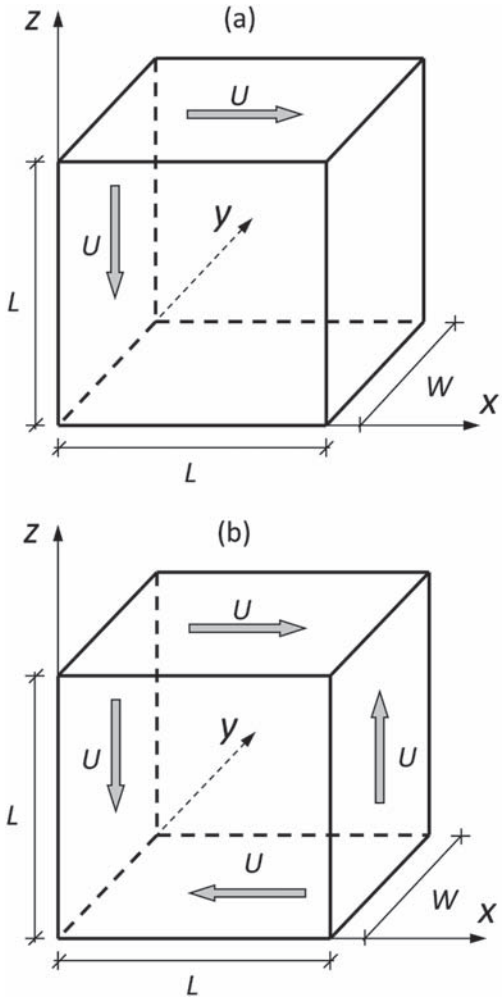

Figure 2. Schematic shows the 3D cavity flow driven by different number of moving walls along the cavity (the same symbol U means they are the same). (a) Two-sided lid (TSL) driven cavity flow, and (b) Four-sided lid (FSL) driven cavity flow. The notations L, W, and L indicate the length, width, and height, respectively. The effects of four different aspect ratios, $K = W/L = 0.25$, 0.5, 0.75 and 1, are studied.

2.2. Boundary condition

Since the 3D lid driven flow is performed in this study, the velocity boundary condition for the moving walls is provided by bouncing the incoming PDFs back to its original position with the additional momentum transfer, i.e., the modified link bounce back boundary condition (d'Humières *et al* 2002)

$$f_{\bar{\alpha}} = f_{\alpha} + 2\omega_{\alpha}\rho_0 \frac{\boldsymbol{e}_{\bar{\alpha}} \cdot \boldsymbol{U}_{\mathrm{lid}}}{c_s^2}, \tag{8}$$

where $f_{\bar{\alpha}}$ is the PDF of $\boldsymbol{e}_{\bar{\alpha}} = -\boldsymbol{e}_{\alpha}$, $\boldsymbol{U}_{\mathrm{lid}}$ stands for the velocity on the moving walls, e.g., the lid speed. For the other stationary walls, the no-slip zero boundary conditions based on the

Table 1. Lattice nodes adopted in the 3D one-sided, two-sided, and four-sided LDC simulations with various aspect ratios at the steady solution for different *Re*.

Re	$K = 0.25$ (L_x, L_y, L_z)	$K = 0.5$ (L_x, L_y, L_z)	$K = 0.75$ (L_x, L_y, L_z)	$K = 1$ (L_x, L_y, L_z)
(one-sided) 400				(96, 96, 96)
1000				(128, 128, 128)
(two-sided) 500	(96, 24, 96)	(112, 56, 112)	(128, 96, 128)	(128, 128, 128)
(four-sided) 300	(128, 32, 128)	(96, 48, 96)	(112, 84, 112)	(112, 112, 112)

mid-grid bounce back approach are applied, i.e., the physical boundary is specified in the middle of the fluid nodes and the inner fictional ghost nodes.

3. Results and discussions

In this section, the MRT-LBE model is validated first by applying it to two published studies of 3D LDC. One is the classical benchmark case, i.e., one-sided LDC, and the other is a TSNFL cavity flow, as shown in figure 2(a). Then, the FSL cavity flow (figure 2(b)) is investigated numerically. We also discuss the grid system adopted for all the simulations, the grid independence study, and the results of the 3D FSL cavity flow with various transverse aspect ratios.

3.1. Grid independence study

In order to correctly simulate the incompressible fluid flows (Mach number $Ma = U/c_s < 0.3$) and to satisfy the numerical stability limitation (the dimensionless relaxation time τ should be sufficiently larger than 0.5), the dimensionless lid driven velocity $U = 0.1$ was chosen for all moving boundary in all the simulations. Based on optimizing the linear stability of the D3Q19 model (d'Humières *et al* 2002), the nineteen elements s_i of the collision matrix other than s_υ are given by: $s_0 = s_3 = s_5 = s_7 = 0$, $s_1 = 1.19$, $s_2 = s_{10} = s_{12} = 1.4$, $s_4 = s_6 = s_8 = 1.2$, $s_{16} = s_{17} = s_{18} = 1.98$, and $s_9 = s_{11} = s_{13} = s_{14} = s_{15} = 1/\tau$. As shown in table 1, the number of the lattice size (L_x, L_y, L_z) adopted in the *x*-, *y*- and *z*-direction changes with the various transverse aspect ratios $K = W/L$ as well as the Reynolds number $Re = UL/\upsilon$. In additional, the steady solution of the laminar flow is determined by the following criterion, i.e., the relative error of velocity at two time-levels separated by *n* (=1000) time steps decreases to the magnitudes of 10^{-8} or less,

$$\sqrt{\sum\left[\frac{(u_i^n - u_i^{n-1})^2 + (v_i^n - v_i^{n-1})^2 + (w_i^n - w_i^{n-1})^2}{(u_i^n)^2 + (v_i^n)^2 + (w_i^n)^2}\right]} \leqslant 10^{-8}. \tag{9}$$

Results of the grid independence study for the 3D one-sided ($Re = 1000$) and two-sided ($Re = 500$) LDC with the aspect ratio $K = 1$ are provided in table 2. The minimum magnitude of the velocity ($u_{\min}$) and the corresponding position ($z_{\min}$) where the $u_{\min}$ occurs are compared between two different grid systems to check the difference. Here we observe that the differences between 128^3 and 144^3 lattice sizes in computing results are about 0.5%, and thus, conclude that the grid size has no noticeable effect on model convergence. Here we only discuss the grid independent on 3D one-and two-sided LDC, and 3D FSL will be given later, in the 3.3 section.

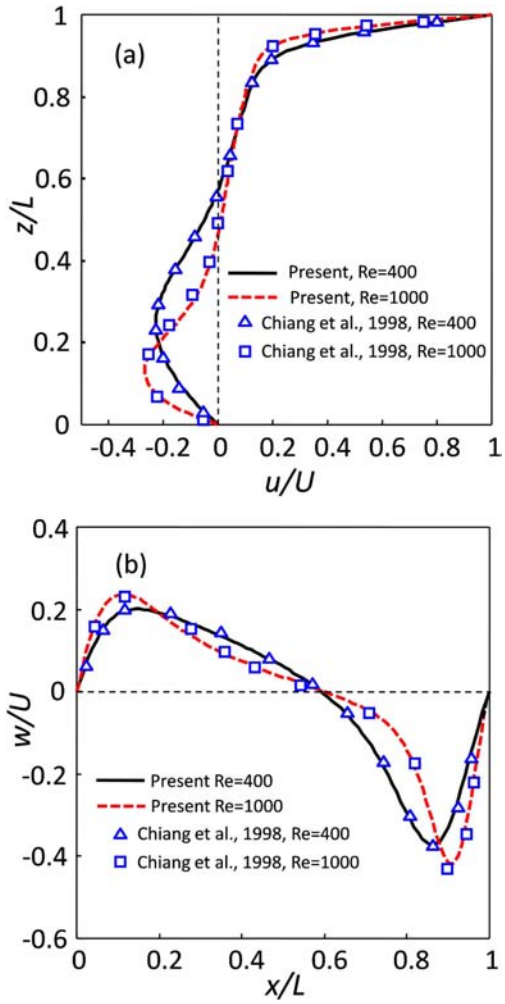

Figure 3. Results of the simulated 3D one-sided LDC at $Re = 400$ and 1000. (a) Horizontal velocity profiles at $x = L/2$ on the symmetry plane, $y = W/2$, and (b) vertical velocity profiles at $z = H/2$ on the mid-plane $y = W/2$.

3.2. Validation of present algorithm

For the one-sided cavity flow, two Reynolds numbers are selected: 400 and 1000 with $K = 1$. The horizontal and vertical velocity profiles, normalized by the reference velocity, on the symmetry plane $y = W/2$, agree very well with those by solving the Navier–Stokes (NS) equation (figure 3) given by Chiang *et al* (1998). The other test case is a 3D two-sided LDC with $K = 1$, 0.75, 0.50, and 0.25 at the same $Re = 500$ (see figure 4) which also indicates an excellent agreement. The curvature of velocity profiles decreases with the aspect ratio, this means the kinetic energy is less transmitted from the driven walls to the cavity center, caused by the fact that a small aspect ratio means a small contact surface, and hence, fewer driven fluid particles, and finally a decrease of the kinetic energy transfer. It is also possible to explain that this is because of the drag effect caused by the stationary end walls. Also, these comparisons with the streamline plot provided by (Oueslati *et al* 2011) are excellent at the

Table 2. Grid independency study for 3D one-sided and two-sided LDC with $K = 1$. Here the $u_{\min}$ stands for the minimum magnitude of horizontal velocity on the symmetry plane, $y = W/2$, and the $z_{\min}$ corresponds to the position where $u_{\min}$ occurs.

		Resolution (Lattice nodes)		
		(96, 96, 96)	(128, 128, 128)	(144, 144, 144)
One-sided	$u_{\min}$	−0.265 662	−0.269 319	−0.270 684 902
($Re = 1000$)	$z_{\min}$	0.130 208 33	0.128 906 25	0.128 472 222
Two-sided	$u_{\min}$	−0.257 376	−0.259 930 864	−0.260 692 779
($Re = 500$)	$z_{\min}$	0.588 541 67	0.582 031 25	0.579 861 111

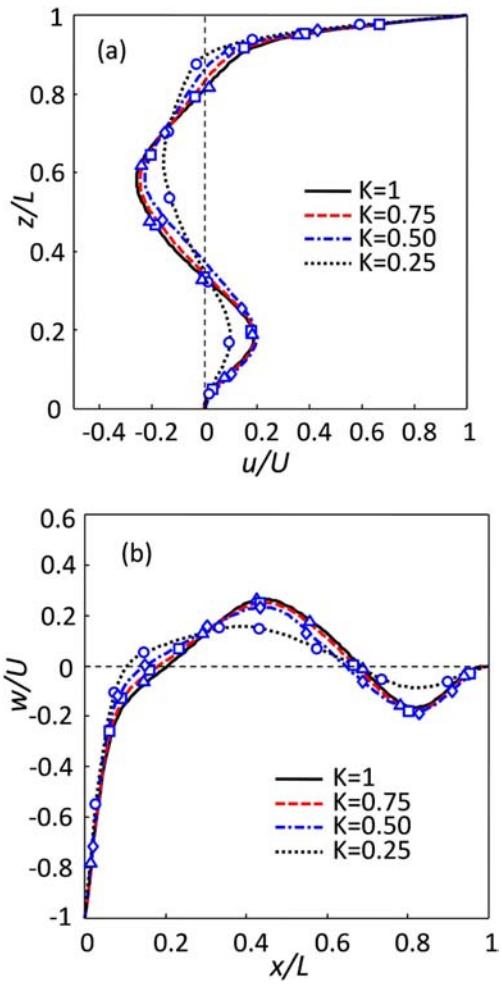

Figure 4. Comparison of present simulated results (lines) of 3D TSNFL for different aspect ratios at $Re = 500$ with the numerical results given by Oueslati *et al* (2011) (Δ : $K = 1$, $\square$: $K = 0.75$, $\diamond$: $K = 0.50$, and $\bigcirc$: $K = 0.25$). (a) Horizontal velocity profiles at $x = L/2$ on the symmetrical plane, $y = W/2$, and (b) vertical velocity profiles at $z = H/2$ on the symmetrical plane $y = W/2$.

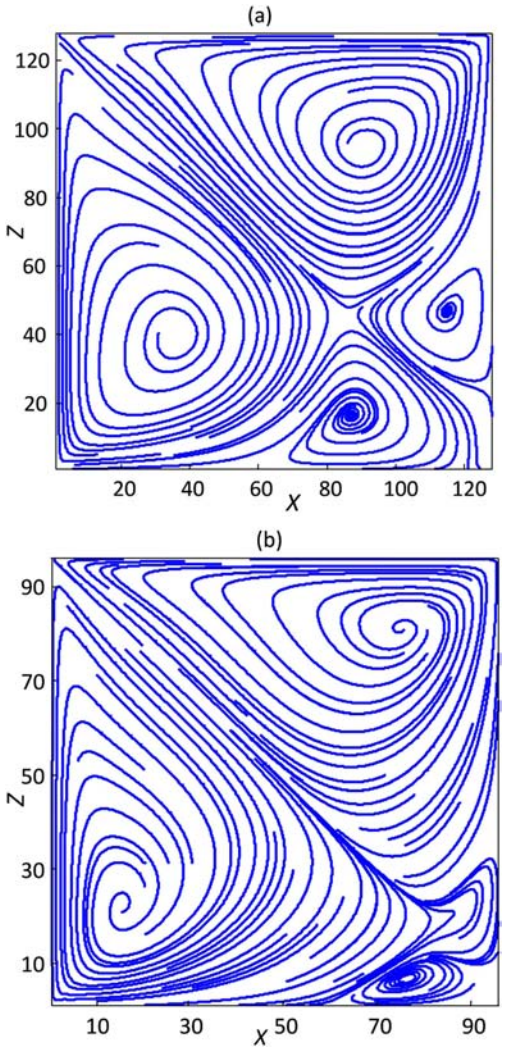

Figure 5. Streamlines of the 3D TSNFL for different aspect ratios on the symmetry plane $y = W/2$ at Re $= 500$, (a) $K = 1$, and (b) $K = 0.25$. The broken of some streamlines is due to the 3D nature. In other words, a streamline goes into (or comes from) the other plane.

various aspect ratio with $Re = 500$. Two examples of this study simulated streamline plot are given in figure 5 as the evidence. With the decrease in aspect ratio K, the central locations of the two primary vortices move closer to the upper right and bottom left corner points, and the two secondary vortices approach to the bottom right corner points.

3.3. Three-dimensional four-sided lid (3D FSL) driven cavity flow

At Re $= 300$, the effects of transverse aspect ratio on the modeled 3D FSL flows at the steady status are present with four ratios, $K = 1$, 0.75, 0.5, and 0.25. The independent grid system can be demonstrated by the negligible small difference (0.5%) for $u_{\min}|[z/L > 0.5]$ which

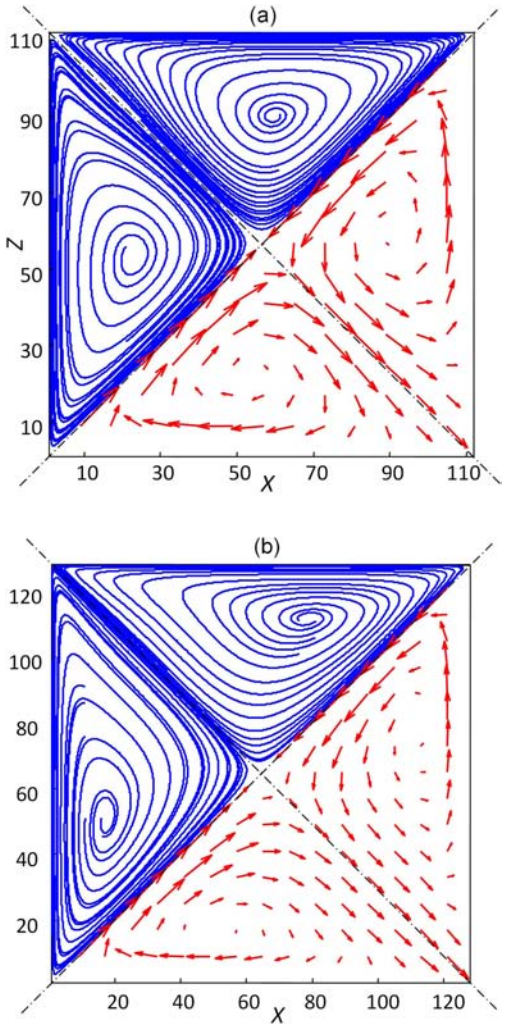

Figure 6. Streamlines and velocity vectors (arrows) on the symmetry plane $y = W/2$ of the 3D FSL cavity flow at $Re = 300$ with different transverse aspect ratios. (a) $K = 1$ and (b) $K = 0.25$. These are similar to the unstable symmetric solution obtained by other 2D simulations that solve the NS equation. Since the flow is symmetrical with respect to the cavity center, only half of the results are plotted.

stands for the minimum magnitude of horizontal velocity for all z/L that are larger than 0.5 and $u_{\max}|[z/L < 0.5]$ which presents the maximum magnitude of horizontal velocity for all z/L that are less than 0.5 (see figure 8).

Four primary vortices are formed with the symmetric patterns about the two cavity diagonals (i.e., the center of cavity) on the mid-plane, $y = W/2$ (figure 6). It clearly shows that the changing of the aspect ratio, i.e., from $K = 1$ to $K = 0.25$, affects the central location of the vortices. The centers of the four vortices move out towards the upper corner and bottom left corners as the decrease of K.

At $Re = 300$, the current 3D MRT-LBE model can only simulate the unstable symmetric solution produced by other 2D modeling (Wahba 2009). Although other 2D LBE modeling

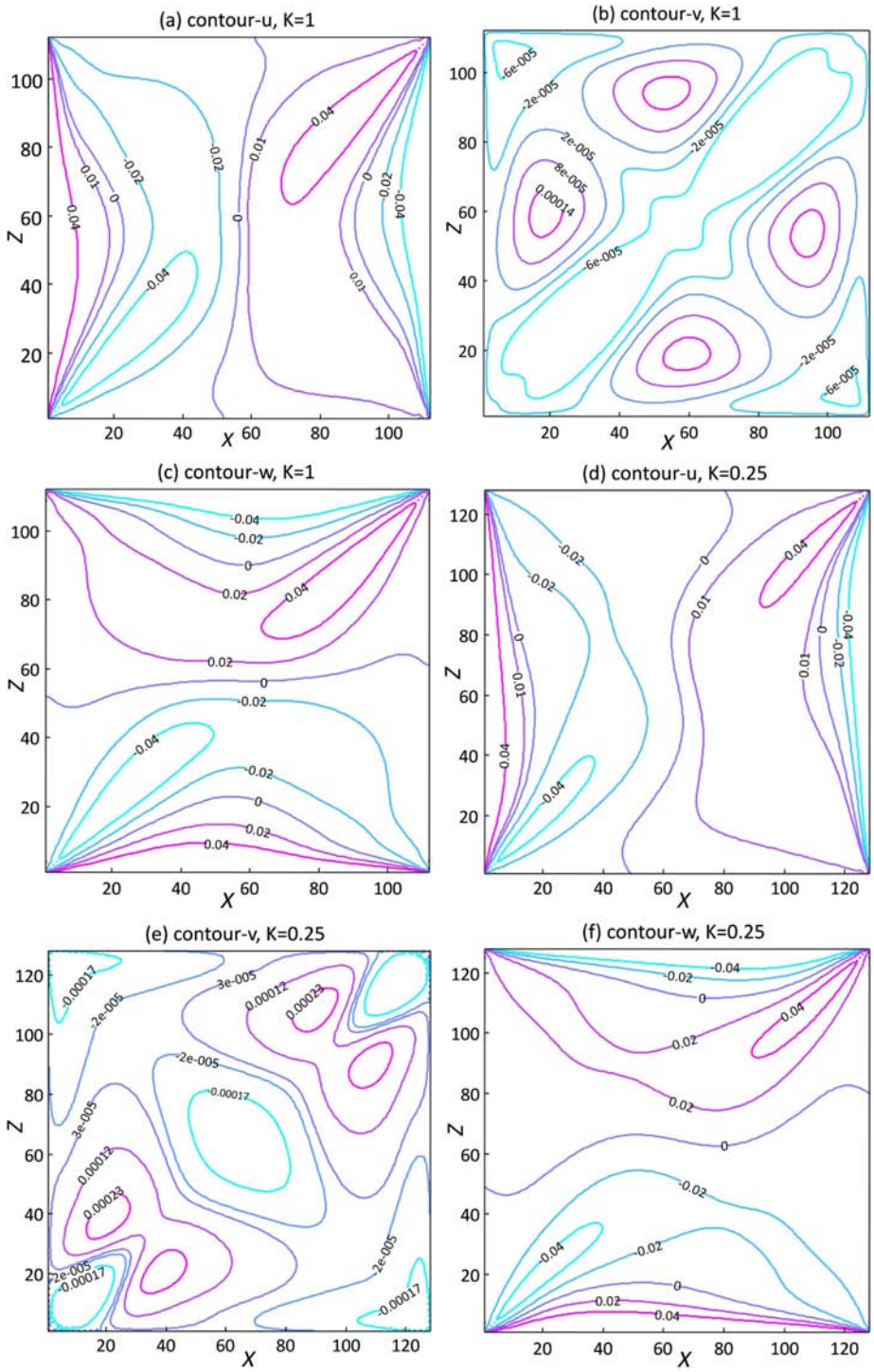

Figure 7. Contours of the horizontal u, transverse v, and vertical w velocity components for different aspect ratios ($K = 1$ and $K = 0.25$) at $Re = 300$ on the symmetry plane, $y = W/2$.

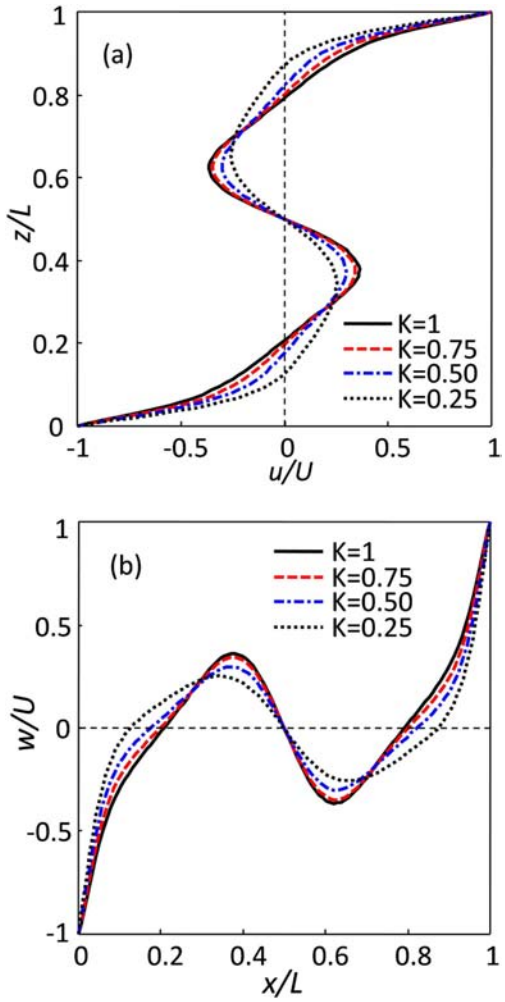

Figure 8. Simulated 3D FSL flow velocity profiles for different aspect ratios at $Re = 300$. (a) Horizontal velocity profiles at $x = L/2$ on the symmetry plane, $y = W/2$, and (b) vertical velocity profiles at $z = H/2$ on the mid-plane $y = W/2$.

results (Perumal and Dass 2011) which has a single relaxation time could obtain the multiple solutions when the Reynolds number is fixed at 300, it may be caused by the stability effect from the end stationary walls available in these 3D modeling effects. More discussion on the multiple flow solutions for 3D FSL flow will be presented later.

The change of aspect ratio K also affects the u, v, w velocity components on the mid-plane, $y = W/2$ (figure 7), especially the v component. With $K = 1$, model simulated v component is the most strongest, among other K values. Contours of v component show 8 vortices (six primary and two secondary vortices formed with symmetric patterns) on the mid-plane, $y = W/2$. When K decreases to 0.25, it shows a total of 9 vortices. The two primary vortices along the anti-diagonal direction are divided into three small vortices, and the other primary vortices move closer to each other. In additional, the horizontal and vertical velocity profiles on the symmetry plane, $y = W/2$, are also influenced by the aspect ratio (figure 8).

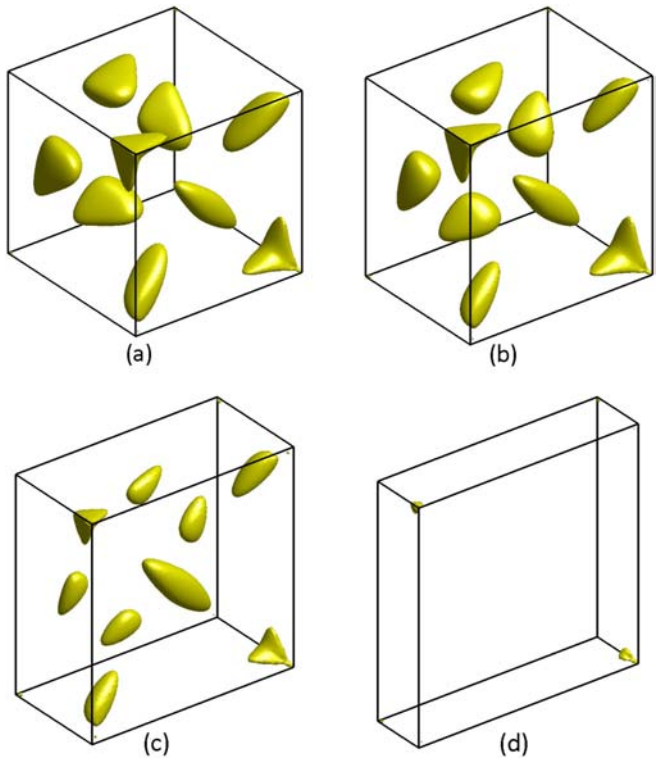

Figure 9. Iso-surface of the transverse velocity component v for the specific value ($v = -0.06$) for different aspect ratios, $K = 1$, 0.75, 0.50, and 0.25 (from (a) to (d)) at $Re = 300$.

As the decrease of the aspect ratio from $K = 1$ to $K = 0.25$, the reducing tendency in the iso-surface of the transverse velocity component, v, for the specific value (-0.06) at $Re = 300$ can be observed in figure 9. It shows that the small aspect ratio ($K = 0.25$) limits the transfer of momentum from the moving lid into the cavity. As an extreme case for $K = 0$, there should have no any velocity at all in the cavity. The decreasing of K practically boosts the importance of the stationary end walls, which pose a drag force on the fluid motion inside the cavity. Here the iso-surface of kinetic energy, defined as $Ke = 0.5(|u|^2 + |v|^2 + |w|^2)$, also demonstrate the stationary end walls effect (figure 10).

3.4. Multiple steady solutions

It was pointed out in previous section that at $Re = 300$ current MRT-LBE model will not produce multiple solutions at steady state for 3D FSL flows. Multiple steady state solutions, however, can be reproduced at different Re's for different aspect ratios. Here let's define the critical Reynolds number (Re_c) is the value for a FSL cavity flow to develop multiple steady solutions when $Re > Re_c$.

For MRT-LBM, the multiple steady solutions could be obtained by (1) changing the Reynolds number, or (2) a slight change of the relaxation time when Re is close to Re_c (Perumal and Dass 2011). For the first approach calculations are performed for the Reynolds varies from 100 to 400, and using a 112^3 grid size with $K = 1$. When $Re \leqslant 380$, the

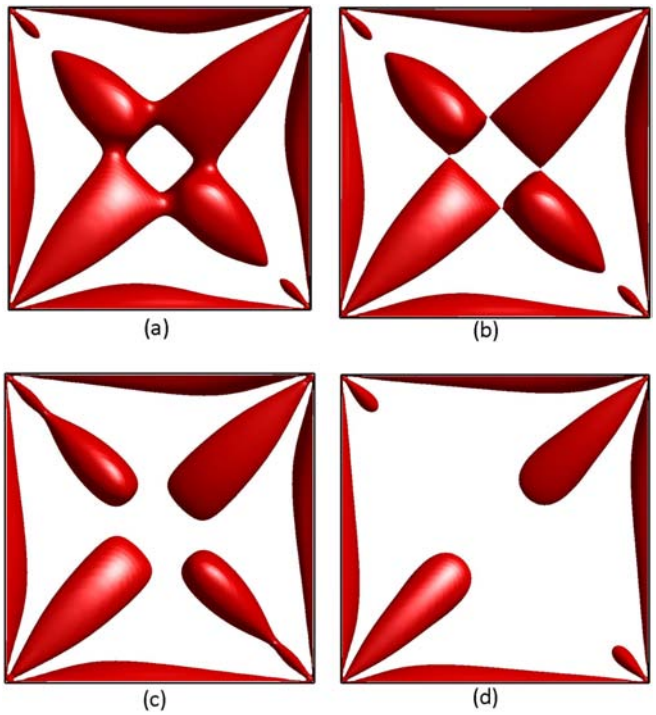

Figure 10. Iso-surface of the kinetic energy ($Ke = 0.06$) for the different aspect ratios, $K = 1$, 0.75, 0.50, and 0.25 (from (a) to (d)) at the middle plane for $Re = 300$.

streamlines of 3D FSL flow are affected slightly by the different Reynolds number, but basically it is maintaining the unstable symmetric pattern, as shown in figure 11(a). When $Re = 381$, the flow structure shows the bifurcation from the symmetry state to the asymmetry state (figure 11(b)). Thus, the critical Reynolds number (Re_c) for 3D FSL with $K = 1$ is identified as 380. This result is different with that observed from the 2D FSL study ($Re_c = 300$) (Wahba 2009, Perumal and Dass 2011), which may be caused by the stability effect from stationary end walls available in this 3D model.

Two possible asymmetry steady solutions at $Re = 381$ (figures 11(b) and 12) show the effect of a slight change of the relaxation time and viscosity, by slightly changing the non-dimensional lid speed. These streamline patterns, however, are similar to these results given by other 2D FSL at $Re = 300$ (Wahba 2009, Perumal and Dass 2011).

For the reduced aspect ratio, i.e., $K = 0.75$, 0.50 and 0.25, the lattice size on y-direction will be decreased, and the numbers of lattices on x- and z-direction are unchanged. The corresponding critical Reynolds numbers at different transverse aspect ratio are plotted in figure 13. It can be seen that the Re_c decreases with increasing aspect ratio, K, and it has a obvious tendency that the critical Reynolds number of 3D FSL will be gradually close to $Re = 300$ for 2D FSL with the increase of K. The possible reason of this phenomenon may be attributed to the fact that the wall effect (when K is small) can maintain the unstable flow pattern with a high Reynolds number. With K increasing, the end wall effect is less important, and thus, Re_c decreases. For this reason, two large transverse aspect ratios, $K = 2$ and 3 are added for further checking this hypothesis. The corresponding grid resolutions are set as ($112 \times 224 \times 112$) and ($112 \times 336 \times 112$), respectively. For $K = 2$, the critical Reynolds

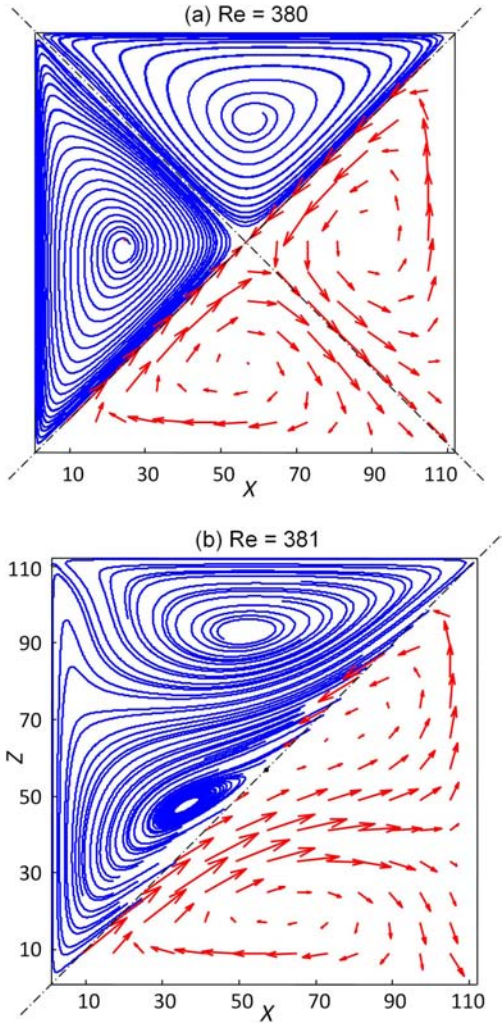

Figure 11. Streamlines and velocity vectors (arrows) of 3D FSL cavity flow with $K = 1$ near the critical Reynolds number, Re_c, the reference lid driven velocity U is chosen as 0.1.

number is 325, and $Re_c = 319$ is captured for $K = 3$. Here it demonstrates Re_c of 3D FSL becomes more and more close to $Re = 300$ for 2D FSL. As well documented for having a negligible end wall effect at the center plane, an aspect ratio of 5 is necessary (Chow 1959). Unfortunately, it is impossible to extend $K \geqslant 4$ because of the limitation on our current computing resources. Nevertheless, results of this study also support a minimum aspect ratio of 5 is required.

4. Conclusions

In this study, the 3D FSL cavity flow has been investigated numerically for analyzing the effects of the transverse aspect ratio on the flow structure by using MRT-LBE with nineteen

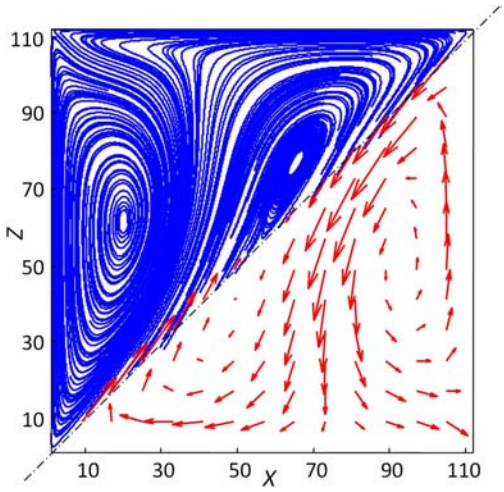

Figure 12. Second steady solution (streamlines and velocity vectors) for 3D FSL cavity flow at $Re = 381$ with the aspect ratio $K = 1$, the reference lid driven velocity U is set equal to 0.09 for another asymmetry solution. The first asymmetry, steady solution is shown as figure 11(b). All figures are symmetric with respect to the cavity center, at grid (61, 61).

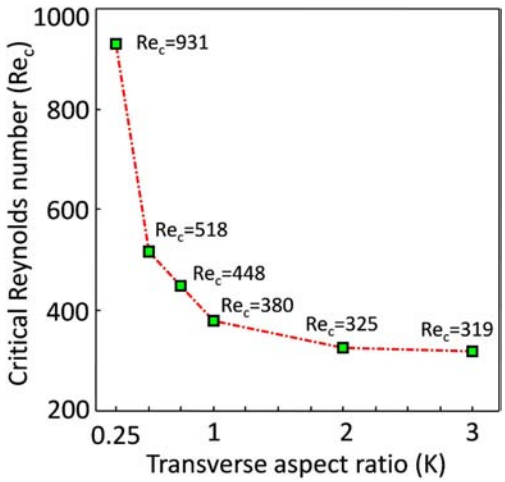

Figure 13. The relationship between the critical Reynolds number (Re_c) and the transverse aspect ratio.

velocity directions model. The flow structure of the 3D FSL cavity flow in the steady state at $Re = 300$ with various transverse aspect ratio, i.e., $K = 3, 2, 1, 0.75, 0.50$ and 0.25, has been described. The streamlines and velocity vectors on the mid-plane, $y = W/2$, demonstrate the presence of four primary vortexes with the symmetric patterns with respect to the two cavity diagonals (i.e., the cavity center) for all K values.

When Reynolds number exceeds a critical value, the instabilities arise and this leads to the flow field changed from symmetry to asymmetry, i.e., the flow bifurcation occurs. By slightly changing the reference velocity for a slightly different relaxation time near the critical

Reynolds number, the two asymmetry steady solutions of 3D FSL cavity flow could be reproduced by this MRT-LBE model. In additional, the critical Reynolds number of 3D modeling is very different from other 2D modeling results, it must be caused by the effect of stationary end walls.

Acknowledgments

The authors would like to thank Dr L S Luo for providing the initial MRT-LBE CPU code. This work is mainly supported by the Virginia Institute of Marine Science, college of William and Mary (VIMS) for the study environment. We also thank Dr J Shen for his great help at VIMS. Supports from the National Natural Scientific Foundation of China with Grant No. 50679008 and 41206075 are also acknowledged.

References

Albensoeder S, Kuhlmann H C and Rath H J 2001 Multiplicity of steady two-dimensional flows in two-sided lid-driven cavities *Theor. Comp. Fluid Dyn.* **14** 223–41

Beya B B and Lili T 2008 Three-dimensional incompressible flow in two-sided non-facing lid-driven cubical cavity *C. R. Mec.* **336** 863–72

Blohm C H and Kuhlmann H C 2002 The two-sided lid-driven cavity: experiments on stationary and time-dependent flows *J. Fluid Mech.* **450** 67–95

Burggraf O R 1966 Analytical and numerical studies of the structure of steady separated flows *J. Fluid Mech.* **24** 113–51

Cadou J M, Guevel Y and Girault G 2012 Numerical tools for the stability analysis of 2D flows: application to the two- and four-sided lid-driven cavity *Fluid Dyn. Res.* **44** 1–12

Chiang T P, Shu W H and Hwang R R 1998 Effect of Reynolds number on the eddy structure in a lid-driven cavity *Int. J. Numer. Methods Fluids* **26** 557–79

Chow V T 1959 *Open-Channel Hydraulics* (New York: McGraw-Hill)

d'Humières D 1992 Generalized lattice Boltzmann equations *Prog. Astron. Aeronaut.* **159** 458–459

d'Humières D, Ginzburg I, Krafczyk M, Lallemand P and Luo L S 2002 Multiple-relaxation-time lattice Boltzmann models in three dimensions *Philos. Trans. R. Soc.* A **360** 437–51

De S, Nagendra K and Lakshmisha K N 2009 Simulation of laminar flow in a three-dimensional lid-driven cavity by lattice Boltzmann method *Int. J. Numer. Methods* H **19** 790–815

Dardis O and Mccloskey J 1998 Lattice Boltzmann scheme with real numbered solid density for the simulation of flow in porous media *Phys. Rev.* E **57** 4834–7

Hou S L, Zou Q S, Chen S, Doolen G and Cogley A C 1995 Simulation of cavity flow by the lattice Boltzmann method *J. Comput. Phys.* **118** 329–47

Hou S L, Sterling J, Chen S and Doolen G D 1996 A lattice Boltzmann subgrid model for high Reynolds number flows *Pattern Formation Lattice Gas Autom.* **6** 151–68 https://arxiv.org/abs/comp-gas/9401004v1

Ghia U, Ghia K N and Shin C T 1982 High-*Re* solutions for incompressible flow using the Navier–Stokes equations and a multigrid method *J. Comput. Phys.* **48** 387–411

Guermond J L, Migeon C, Pineau G and Quartapelle L 2002 Start-up flows in a three-dimensional rectangular driven cavity of aspect ratio 1:1:2 at $Re = 1000$ *J. Fluid Mech.* **450** 169–99

Gunstensen A K, Rothman D H, Zaleski S and Zanetti G 1991 Lattice Boltzmann model of immiscible fluids *Phys. Rev.* A **43** 4320–7

Koseff J R and Street R L 1984a Visualization studies of a shear driven three-dimensional recirculating flow *J. Fluid. Eng.* **106** 21–9

Koseff J R and Street R L 1984b On end wall effects in a lid-driven cavity flow *J. Fluid. Eng.* **106** 385–9

Koseff J R and Street R L 1984c The lid-driven cavity flow: a synthesis of qualitative and quantitative observations *J. Fluid. Eng.* **106** 390–8

Kuhlmann H C, Wanschura M and Rath H J 1997 Flow in two-sided lid-driven cavities: non-uniqueness, instabilities, and cellular structures *J. Fluid Mech.* **336** 267–99

Lallemand P and Luo L S 2000 Theory of the lattice Boltzmann method: dispersion, dissipation, isotropy, galilean invariance, and stability *Phys. Rev.* E **61** 6546–62

Li C G, Maa J P Y and Kang H G 2012 Solving generalized lattice Boltzmann model for 3D cavity flows using CUDA-GPU *Sci. China Phys. Mech. Astron.* **55** 1894–904

Oueslati F, Beya B B and Lili T 2011 Aspect ratio effects on three-dimensional incompressible flow in a two-sided non-facing lid-driven parallelepiped cavity *C. R. Mec.* **339** 655–65

Pan F and Acrivos A 1967 Steady flows in rectangular cavities *J. Fluid Mech.* **28** 643–55

Perumal D A and Dass A K 2011 Multiplicity of steady solutions in two-dimensional lid-driven cavity flows by lattice Boltzmann method *Comput. Math. Appl.* **61** 3711–21

Prasad A K and Koseff J R 1989 Reynolds number and end-wall effects on a lid driven cavity flow *Phys. Fluids* A **1** 208–18

Shankar P N and Deshpande M D 2000 Fluid mechanics in the driven cavity *Annu. Rev. Fluid Mech.* **32** 93–136

Succi S 2001 *The Lattice Boltzmann Equation for Fluid Dynamics and Beyond* (Oxford: Oxford University Press)

Wahba E M 2009 Multiplicity of states for two-sided and four-sided lid driven cavity flows *Comput. Fluids* **38** 247–53